Available online at www.sciencedirect.com
SCIENCE DIRECT®
Journal of Solid State Chemistry 178 (2005) 1935–1939
JOURNAL OF SOLID STATE CHEMISTRY
www.elsevier.com/locate/jssc

Structure and magnetic properties of $Ca_{14}MnP_{11}$

Hyungrak Kim, Susan M. Kauzlarich*

Department of Chemistry, University of California, One Shields Avenue, Davis, California 95616, USA

Received 26 January 2005; received in revised form 25 March 2005; accepted 27 March 2005
Available online 27 April 2005

Abstract

The compound $Ca_{14}MnP_{11}$ crystallizes in the $Ca_{14}AlSb_{11}$ structure type with the tetragonal space group $I4_1/acd$ ($Z = 8$) and lattice parameters of $a = 15.3255(7)$ Å, $c = 20.7565(9)$ at 90 K. The structure consists of MnP_4^{9-} tetrahedron, P_3^{7-} trimer, 4 P^{3-} isolated anions and 14 Ca^{2+} cations. Similar to other compounds of this structure type containing phosphorous, the P_3^{7-} trimer has a central P atom that is best modeled in the structure as being equally split between two sites. In addition, there is no additional distortion of the manganese-containing tetrahedron compared with the main group analog, $Ca_{14}GaP_{11}$, suggesting that the Mn oxidation state is Mn^{2+}. Temperature-dependent magnetic susceptibility shows that the compound is paramagnetic over the entire temperature range measured (2–300 K). The data can be fit with a modified Curie–Weiss law and provide an effective magnetic moment of 5.80 (2) B.M. with a Weiss constant of −2.13(2) K and $\chi_0 = -9(1) \times 1^{-5}$ emu/mol. This moment is significantly higher than those measured for any of the Mn-containing analogs and is consistent with Mn^{2+}. This result will be discussed in light of the electron counting scheme for Mn compounds of the $Ca_{14}AlSb_{11}$ structure-type.

Keywords: Magnetic material; Zintl compound; Synthesis of new compound; Magnetic Zintl phase; $Ca_{14}AlSb_{11}$ structure type

1. Introduction

Manganese-containing compounds of the $Ca_{14}AlSb_{11}$ structure type [1] exhibit novel magnetic and electronic properties [2–4]. In general, the structure can be understood within the Zintl formulism as composed of $AlSb_4^{9-}$ tetrahedron, Sb_3^{7-} trimer, 4 Sb^{3-} anions, and 14 Ca^{2+} cations. The main group-containing compounds are semiconductors and the Mn-containing compounds show unusual behavior such as long-range magnetic ordering and colossal magnetoresistance [5–12]. These magnetic properties are surprising considering that there are no possible mechanisms for orbital super-exchange and the tetrahedron are well separated. However, the magnetic ordering can be correlated with metallicity and Mn–Mn distance in these compounds, suggesting that the magnetic interactions can be attributed to a Ruderman–Kittel–Kasuya–Yosida (RKKY) type model [2].

These compounds have been referred to as transition metal Zintl compounds and the electron book keeping to account for formal oxidation states is suggested to be the same as that provided for the main group elements. In the series, $Ca_{14}MnPn_{11}$ (Pn = As, Sb, Bi), the As compound shows paramagnetic behavior consistent with Mn^{3+} over all temperatures. The Sb and Bi compounds are ferromagnetic at 65 and 55 K, respectively [2]. This high-temperature magnetic ordering is unusual. Other transition metal Zintl phases synthesized with Nb as the transition metal do not show ferromagnetic ordering [13–16].

The magnetism, reported to date, of all the Sb and Bi compounds of the $Ca_{14}AlSb_{11}$ structure type containing Mn is consistent with 4 unpaired electrons being present on the Mn, suggesting a valence of d^4. This is a highly unusual oxidation state for Mn in a tetrahedral coordination [17]. The tetragonal distortion of the Mn tetrahedron compared to the main group analogs was

*Corresponding author. Fax: +1 530 752 8995.
E-mail address: smkauzlarich@ucdavis.edu (S.M. Kauzlarich).

0022-4596/$ - see front matter © 2005 Elsevier Inc. All rights reserved.
doi:10.1016/j.jssc.2005.03.041

deemed supporting evidence for the oxidation state. Recent theoretical studies [18] on the metallic compounds, $Ca_{14}MnBi_{11}$ and $Ba_{14}MnBi_{11}$, suggest that the electron counting be re-evaluated and postulates that charge balance is maintained if the tetrahedral unit be considered to be $Mn^{2+}(Bi_4)^{11-}$ rather than $Mn^{3+}(Bi_4)^{12-}$. X-ray Magnetic Circular Dichroism (XMCD) experimental spectra [19] for $Yb_{14}MnSb_{11}$ shows that in this compound, Mn is best considered to be Mn^{2+} with an antiferromagnetically coupled spin on Sb [19]. ESR measurements on $Ca_{14}AlP_{11}$ show no signal, as expected from the Zintl electron counting, and $Ca_{14}MnP_{11}$ show a broad signal at $g = 2.00$, suggesting uncompensated spin density [20].

EPR and ^{31}P solid-state NMR on $Ca_{14}MnP_{11}$ has been published [20]. That paper investigated the structural status of the P_3 trimer. In this paper, we report the synthesis and structure of the compound, $Ca_{14}MnP_{11}$, which crystallizes in the $Ca_{14}AlSb_{11}$ structure type, along with its temperature-dependent magnetization data.

2. Experimental procedures

Synthesis. Ca metal was obtained (J. Matthey, 99.99%) and cut into small pieces. Red phosphorus (J. Matthey, 99.9999%) was used as received. Mn flakes (J. Matthey, 99.98%) were first cleaned in a 5% HNO_3/CH_3OH solution, transferred into a drybox and ground into a powder. All materials were handled in an argon drybox. $Ca_{14}MnP_{11}$ (powder/single crystal) was prepared by weighing stoichiometric amounts of the elements in a drybox and loading into a clean tantalum tube with a sealed end and subsequently sealing in an argon-filled arc welder. Ta tubes had been cleaned prior to arc welding with 20% HF, 25% HNO_3, and 55% H_2SO_4 solution. The sealed Ta tube was further sealed in a fused silica tube under $\frac{1}{5}$ atmosphere purified argon. Reflective polycrystalline pieces were obtained by heating the mixtures in a box furnace with $T = 1050\,^{\circ}C$ for 5 days. Single crystal needles (1 mm) were found from the reaction of a zone furnace by heating the mixtures with $T = 1100\,^{\circ}C$ for 10 days. All reactions were opened and examined in a nitrogen-filled drybox equipped with a microscope with water levels less than 1 ppm.

Powder X-ray diffraction. The product purity of powder sample was checked by powder X-ray diffraction data on an Enraf-Nonius Guinier camera equipped with a quartz monochromator that gave Cu$K\alpha_1$ radiation. Powdered silicon (NBS) was included in the samples as an internal standard. The powder diffraction pattern was compared with the calculated pattern based on the single crystal crystallographic data and gave an excellent agreement in 2θ positions and intensities.

Structure determination. The tantalum tube was opened in a drybox equipped with a microscope. Metallic and highly reflective needle crystals (1 mm) were transferred to Exxon Paratone N oil for X-ray structure determination. A suitable crystal ($0.12 \times 0.07 \times 0.07\,mm^3$) was mounted on a thin glass fiber and positioned under a cold stream of N_2 in a Bruker SMART 1000 CCD diffractometer equipped with a CRYO COOLER low temperature apparatus (CRYO INDUSTRIES of America, Inc.). No decomposition of the crystal was observed during data collection. The SMART software [21] was used for data collection and SAINT [22] for data integration. The absorption correction was performed using SADABS. The structure was solved by direct method and refined using SHELXL-97 [23]. Data collection parameters and crystallographic data are provided in Table 1. Further details of the crystal structure investigation can be obtained from the Fachinformationszentrum Karlsruhe, 76344 Eggenstein-Leopoldshafen, Germany, (fax: (49) 7247 808 666; e-mail: crysdata@fiz.karlsruhe.de) on quoting depository number CSD 415071.

Magnetic measurements. DC magnetization data were obtained with a Quantum Design MPMS Superconducting Quantum Interference Device (SQUID) magnetometer with a 7 T superconducting magnet. The data were collected and analyzed with the Magnetic Property Measurement System software supplied by Quantum Design. For single crystal magnetic measurements, the same crystal ($0.80 \times 0.07 \times 0.07\,mm^3$) that was used for the structure determination was placed in a straw. Powdered samples were prepared in a drybox by loading 20 mg into a gel-capsule placed in a straw. The temperature dependence was measured between 5 and

Table 1
Crystal data and structure refinement for $Ca_{14}MnP_{11}$, tetragonal, $I4_1/acd$, $Z = 8$

Formula weight ($g\,mole^{-1}$)	956.73
Temperature (K)	90(2)
Unit cell dimensions (Å)	$a = 15.3255(7)$
	$c = 20.7565(9)$
Volume (Å^3)	4875.1(4)
Density (calculated) (g/cm^3)	2.607
μ Mo$K\alpha$ (mm^{-1})	4.199
θ range	2.66° to 31.49°
Reflections collected	21616
Independent reflections	1998 [R(int) = 0.0523]
Observed reflections ($I > 2\sigma(I)$)	1509
Max. and min. transmission	0.7720 and 0.6262
Data/restraints/parameters	1998/0/63
S (Goodness-of-fit on F^2)	1.258
R indices (all data)[a,b]	$R_1 = 0.0512$, w$R_2 = 0.0818$
Largest diff. peak and hole ($e\,Å^{-3}$)	1.819 and −0.948

[a] $R_1 = \sum||F_o|-|F_c||/\sum|F_o|$.
[b] $wR_2 = [\sum[w(F_o^2\text{-}F_c^2)^2]/\sum[w(F_o^2)^2]]^{1/2}$,
$w^{-1} = [\sigma^2(F_o^2) + (0.0305P)^2 + 28.39P]$, where $P = [\max(F_o^2, 0) + 2F_c^2]/3$.

300 K under 5000 Oe. The field-dependent magnetization was measured between −7 and 7 T at 5 K.

3. Results and discussion

3.1. Structure

The $Ca_{14}AlSb_{11}$ structure type has been well-studied and the phosphorus-containing analogs have been described in detail [5,20,24,25]. $Ca_{14}MnP_{11}$ is the second example of a Mn-containing phosphorus analog, with the only other example being $Eu_{14}MnP_{11}$ which shows ferromagnetic ordering and colossal magnetoresistance [5,20]. The structure of $Ca_{14}MnP_{11}$ will be briefly described and compared to the Eu analog as well as to the main group compounds, $Ca_{14}AlP_{11}$, $Ca_{14}GaP_{11}$, and $Ba_{14}InP_{11}$ [20,24,25]. The compound, $Ca_{14}MnP_{11}$ crystallizes in the space group $I4_1/acd$. $Ca_{14}MnP_{11}$ is isotypic to $Ca_{14}AlSb_{11}$ and part of a family of Mn-containing transition metal Zintl phases. This new phase completes the series of $Ca_{14}MnPn_{11}$, where Pn = P, As, Sb, Bi [26], and has already been studied by wide-line ^{31}P solid-state NMR and EPR [20]. Efforts to prepare large crystals for detailed magnetic and transport properties have been unsuccessful to date. Small single crystals and phase pure powders could be prepared by the stoichiometric reaction of the elements, sealed in a tantalum tube, at high temperatures. The compound is air and water sensitive.

Table 1 lists information pertaining to data collection, data refinement, and the structure solution. Table 2 provides positional parameters. Typically, the description of the structure focuses on the covalently bonded units of this structure type which, in this case, consist of a MnP_4 tetrahedron and a P_3^{7-} linear anion. Fig. 1 shows a view of the structure with the Mn tetrahedra represented as polyhedra and the linear units. The single crystal structures of $Ba_{14}InP_{11}$ [24], $Ca_{14}GaP_{11}$ [25], and $Eu_{14}MnP_{11}$ [5] have been reported. Unit cell parameters for $Ca_{14}AlP_{11}$ have also been reported [20], but single crystals were never isolated and structural parameters were assumed to be the same as $Ca_{14}MnP_{11}$.

Table 2
Atomic coordinates ($\times 10^4$) and equivalent isotropic displacement parameters ($Å^2 \times 10^3$)[a]

	x	y	z	U_{eq}
P(1)	1352(1)	3852(1)	1250	13(1)
P(2)	47(1)	1123(1)	8068(1)	12(1)
P(3)	8719(1)	9739(1)	9533(1)	19(1)
P(4)[b]	209(1)	2709(1)	1250	13(1)
Mn	0	2500	8750	9(1)
Ca(1)	−421(1)	−720(1)	8275(1)	14(1)
Ca(2)	−252(1)	1238(1)	72(1)	17(1)
Ca(3)	3520(1)	0	2500	10(1)
Ca(4)	1764(1)	4020(1)	8447(1)	18(1)

[a] U_{eq} is defined as one third of the trace of the orthogonalized U_{ij} tensor.
[b] Occupancy = 50%.

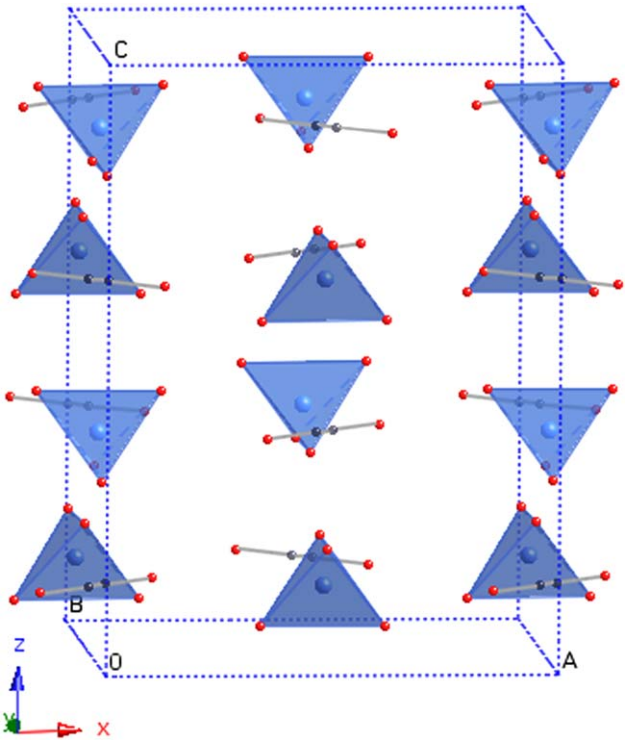

Fig. 1. Unit cell of $Ca_{14}MnP_{11}$ showing the MnP_4 tetrahedra and the Pn_3 trimers. The red balls are P, the gray show P(4) in a disordered position, and blue represent Mn atoms.

All of the phosphides reported to date show a splitting of the central atom of the P_3^{7-} unit in a similar manner, shown in Fig. 2. Table 3 provides selected bond distances and angles. The P(4)–P(4′) distance is 0.906 (4) Å, and the P(1)–P(4) distance is 2.476 (3) Å. The P_3 unit is encased in a cage of cations and is the most distorted in the case of $Ba_{14}InP_{11}$, which also contains the largest cation [24]. In all cases this has been interpreted as statistical disorder of the structure and is represented as a single bonded P_2^{4-} and one distant P^{3-} anion. The model, described as a single bonded P_2^{4-} dumbbell and P^{3-}, statistically disordered in the structure, is supported by IR and Raman spectroscopies for the Ba case [24]. The P_3^{7-} trimer distortion to a single bonded P_2^{4-} dumbbell and P^{3-} is significantly less for either the $Ca_{14}GaP_{11}$ [25] or $Ca_{14}MnP_{11}$ structures and wide-line ^{31}P NMR [20] of $Ca_{14}MnP_{11}$ provides a consistent structural model with the P_3^{7-} unit being trimeric at room temperature.

The mean interatomic distance of P(4)–P(1) is 3.19, 2.99, and 2.93 Å for $Ba_{14}InP_{11}$, $Eu_{14}MnP_{11}$, and $Ca_{14}GaP_{11}$ [5,24,25]. These distances are much larger than the typical single bond length observed in polyphosphides (2.16–2.30 Å) [27], but smaller than the van der

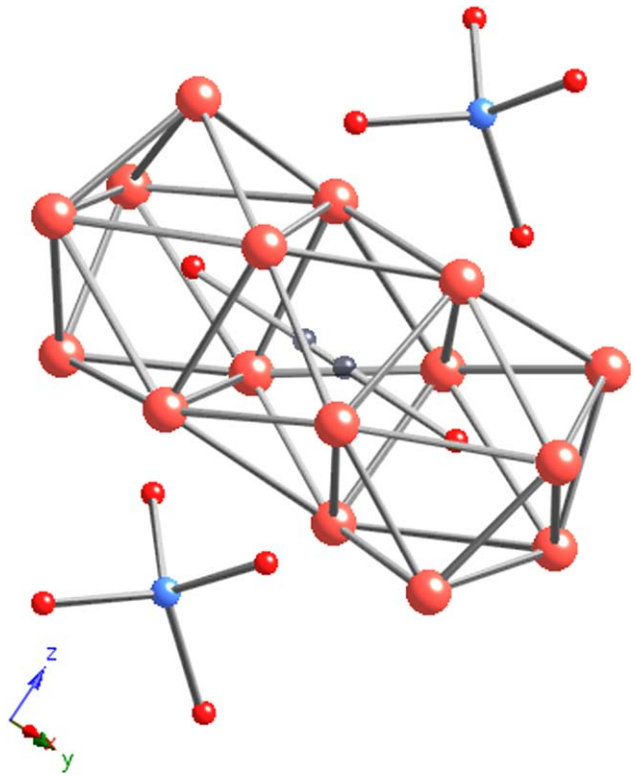

Fig. 2. A view of the asymmetric trimer, P_3, shown with the surrounding cation cage and two neighboring MnP_4 tetrahedra.

Table 3
Selected bond lengths [Å] and angles [°] for $Ca_{14}MnP_{11}$

P(1)–Ca(1)	2.9630(9)
P(1)–Ca(4)	2.9671(11)
P(1)–Ca(2)	2.9731(8)
P(1)–Ca(3)	3.1413(5)
P(2)–Ca(2)	2.8648(10)
P(2)–Ca(4)	2.8929(10)
P(2)–Ca(1)	2.9434(10)
P(2)–Ca(1)	2.9450(10)
P(2)–Ca(3)	3.0282(10)
P(2)–Ca(4)	3.1022(11)
P(2)–Ca(2)	3.4674(10)
P(3)–Ca(3)	2.8781(10)
P(3)–Ca(2)	2.9049(11)
P(3)–Ca(1)	2.9596(11)
P(3)–Ca(2)	3.0037(11)
P(3)–Ca(1)	3.0091(11)
P(3)–Ca(4)	3.0394(11)
P(3)–Ca(4)	3.0471(11)
P(4)–Ca(1)	2.7746(10)
P(4)–Ca(2)	2.9301(11)
P(4′)–Ca(1)	3.2198(15)
P(4)–Ca(2)	3.3996(15)
P(1)–P(4)	2.476(3)
P(4)–P(4′)	0.906(4)
Mn–P(2)	2.5426(8)
P(2)–Mn-P(2)	108.046(17)
P(2)–Mn–P(2)	112.36(4)

Waals distance of approximately 3.60 Å. The P(4)–P(1) distance is the same for both $Ca_{14}MnP_{11}$ and $Ca_{14}GaP_{11}$, consistent with the interpretation that the cations control the distance between P ions. The cation matrix and their electrostatic interactions determine the size of the cavity and the anion adopts this disordered arrangement in order to accommodate the cavity.

The Mn–P(2) distance is slightly smaller (2.5426 (8) Å) than that in $Eu_{14}MnP_{11}$ (2.585 (2) Å), the only other transition metal phosphide with this structure type [5]. This may be attributed to the cation matrix, since this distance is almost the same as the Ga–P(2) distance (2.541(2) Å) observed in $Ca_{14}GaP_{11}$ [25]. The MnP_4 tetrahedron shows a slight distortion away from the ideal tetrahedral angle to 108.0° and 112.4°, which is not as large as that observed for $Eu_{14}MnP_{11}$ (106.6° and 115.4°) [5], but is almost identical to that observed for $Ca_{14}GaP_{11}$ (108.0° and 112.5°) [25]. Mn-containing analogs of the heavier group 15 elements show larger distortions from ideal tetrahedral angles than their corresponding main group analogs [2]. This increased distortion of the tetrahedron for the Mn compounds has been attributed in the past to a Jahn–Teller distortion of a Mn^{3+} ion (d^4 electronic configuration). However; matrix effects, and more subtle bonding requirements, clearly play a role. The fact that there is no difference between tetrahedral angles for the Ga and the Mn-containing compound would be consistent with the oxidation state assignment for Mn in this compound to be most likely Mn^{2+}. No Jahn–Teller distortion is expected for the half-filled electronic configuration of Mn^{2+} (d^5), consistent with the structural data.

3.2. Magnetic measurements

Fig. 3 shows the magnetic susceptibility and inverse susceptibility as a function of temperature for $Ca_{14}MnP_{11}$. $Ca_{14}MnP_{11}$ shows Curie–Weiss behavior over the entire temperature range. The data can be fit with a modified Curie–Weiss law ($\chi = C/(T-\theta)+\chi_0$). The resulting parameters are $\chi_0 = -9(1)\times 10^{-5}$ emu/mol, $C = 4.20(3)$, $\theta = -2.13(6)$ K. The effective moment can be obtained from the Curie constant, C, via the equation $\mu_{eff} = (7{\cdot}999C)^{1/2}$ and is 5.80 (1) μ_B. Unlike $Eu_{14}MnP_{11}$ which shows ferromagnetic ordering and colossal magnetoresistance [5], $Ca_{14}MnP_{11}$ shows none of those properties. Moreover, the moment obtained from the fit of the data is much higher than observed in any other Mn-containing compound in this series [2]. Theoretical calculations [18] for $Ca_{14}MnBi_{11}$ and XMCD measurements [19] on $Yb_{14}MnSb_{11}$ suggest that Mn is Mn^{2+} in these compounds. In the simplist picture, rather than considering the oxidation state on Mn alone, one can consider the cluster $MnPn_4^{9-}$. The assignment of 9− is a result of the Zintl electron counting. The two extremes in charge counting are $Mn^{3+}(Pn_4)^{12-}$ and

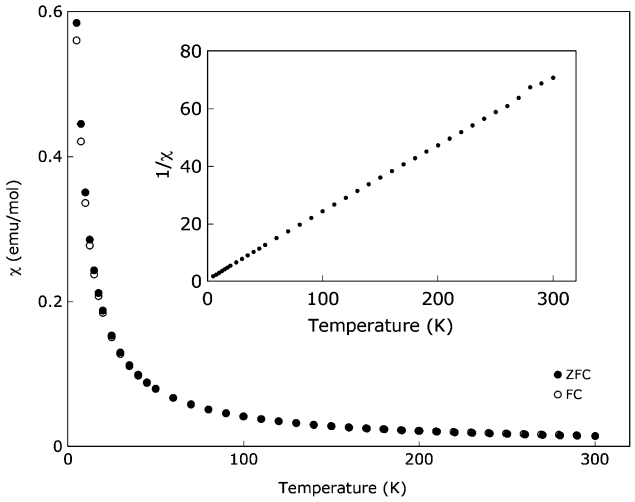

Fig. 3. Magnetic susceptibility (χ) and (inset) inverse susceptibility (χ^{-1}) versus temperature.

$Mn^{2+}(Pn_4)^{11-}$. In the first case there is a hole on the Mn, and all the *Pn* orbitals are filled. In the second case, the Mn orbitals are half filled, and there is a hole on the *Pn* ligands. The magnetic data is more consistent with the electron counting scheme of $Mn^{2+}(Pn_4)^{11-}$.

3.3. Summary

Single crystals of $Ca_{14}MnP_{11}$ have been prepared, and the magnetic susceptibility has been measured. In contrast to Mn compounds of the $Ca_{14}AlSb_{11}$ structure containing heavier pnicogens such as As, Sb, and Bi, there is no distortion of the MnP_4 tetrahedron and the paramagnetic moment is most consistent with Mn^{2+}. This is the first Mn-containing compound of this structure type to unambiguously show that Mn is in the 2+ oxidation state. This provides further validity to the theoretical model proposed for the Bi-containing compounds [18], and incentive to study the magnetic and electronic properties of this family of compounds in more detail.

Acknowledgment

We thank Warren E. Pickett for useful discussion, Robert N. Shelton for the use of the SQUID magnetometer, Amy C. Payne for her contributions to the preliminary stages of this work, and Marilyn M. Olmstead for assistance with crystallography. This research was supported by NSF DMR-9803074, -0120990.

References

[1] G. Cordier, H. Schäfer, M. Stelter, Z. Anorg. Allg. Chem. 519 (1984) 183–188.
[2] S.M. Kauzlarich, A.C. Payne, D.J. Webb, in: J.S. Miler, M. Drillon (Eds.), Magnetism: Molecules to Materials III, Wiley-VCH, Weinheim, 2002, pp. 37–62.
[3] S.M. Kauzlarich, in: S.M. Kauzlarich (Ed.), Chemistry, Structure, and Bonding of Zintl Phases and Ions, VCH Publishers, Inc., New York, 1996, pp. 245–274.
[4] S.M. Kauzlarich, T.Y. Kuromoto, Croat. Chem. Acta 64 (1991) 343–352.
[5] A.C. Payne, M.M. Olmstead, S.M. Kauzlarich, D.J. Webb, Chem. Mater. 13 (2001) 1398–1406.
[6] H. Kim, J.Y. Chan, M.M. Olmstead, P. Klavins, D.J. Webb, S.M. Kauzlarich, Chem. Mater. 14 (2002) 206–216.
[7] H. Kim, M.M. Olmstead, P. Klavins, D.J. Webb, S.M. Kauzlarich, Chem. Mater. 14 (2002) 3382–3390.
[8] J.Y. Chan, S.M. Kauzlarich, P. Klavins, J.-Z. Liu, R.N. Shelton, D.J. Webb, Phys. Rev. B 61 (2000) 459–463.
[9] J.Y. Chan, S.M. Kauzlarich, P. Klavins, R.N. Shelton, D.J. Webb, Phys. Rev. B 57 (1998) 8103–8106.
[10] J.Y. Chan, S.M. Kauzlarich, P. Klavins, R.N. Shelton, D.J. Webb, Chem. Mater. 9 (1997) 3132–3135.
[11] J.Y. Chan, M.E. Wang, A. Rehr, S.M. Kauzlarich, D.J. Webb, Chem. Mater. 9 (1997) 2131–2138.
[12] I.R. Fisher, T.A. Wiener, S.L. Bud'ko, P.C. Canfield, J.Y. Chan, S.M. Kauzlarich, Phys. Rev. B 59 (1999) 13829–13834.
[13] K. Vidyasagar, W. Hönle, H.G. von Schnering, J. Alloys Compd. 236 (1996) 38–41.
[14] K. Vidyasagar, W. Hönle, H.G. von Schnering, Z. Anorg. Allg. Chem. 622 (1996) 518–524.
[15] F. Gascoin, S.C. Sevov, Inorg. Chem. 42 (2003) 8567–8571.
[16] F. Gascoin, S.C. Sevov, Inorg. Chem. 42 (2002) 904–907.
[17] T.Y. Kuromoto, S.M. Kauzlarich, D.J. Webb, Mol. Cryst. Liq. Cryst. 181 (1989) 349–357.
[18] D. Sánchez-Portal, R.M. Martin, S.M. Kauzlarich, W.E. Pickett, Phys. Rev. B 65 (2002) 144414.
[19] A.P. Holm, S.M. Kauzlarich, S.A. Morton, G.D. Waddill, W.E. Pickett, J.G. Tobin, J. Am. Chem. Soc. 124 (2002).
[20] E. Ratai, P. Bruins, C.J. Hernandez, S.M. Kauzlarich, M.P. Augustine, Chem. Mater. 14 (2002) 2467–2475.
[21] SMART, Siemens Analytical X-ray Systems, Inc., Madison, WI, 1994.
[22] SAINT, 6 ed., Siemens Analytical X-ray Systems, Inc., Madison, WI, 1999.
[23] G.M. Sheldrick, 5.10 ed., Bruker AXS Inc., Madison, WI, 1997.
[24] W. Carrillo-Cabrera, M. Somer, K. Peter, H.G. von Schnering, Chem. Ber. 129 (1996) 1015–1023.
[25] J.T. Vaughey, J.D. Corbett, Chem. Mater. 8 (1996) 671–675.
[26] A. Rehr, T.Y. Kuromoto, S.M. Kauzlarich, J. Del Castillo, D.J. Webb, Chem. Mater. 6 (1994) 93–99.
[27] H.G. von Schnering, W. Hölne, Chem. Rev. 88 (1988) 243–273.